Biomedical Journal 47 (2024) 100701

Contents lists available at ScienceDirect

Biomedical Journal

journal homepage: www.elsevier.com/locate/bj

Comprehensive insight into the alterations in the gut microbiome and the intestinal barrier as a consequence of iron deficiency anaemia

Ana Soriano-Lerma [a,b,c], María García-Burgos [a,b], Wiley Barton [d,e], María José M. Alférez [a], Jorge Valentín Crespo-Pérez [f], Miguel Soriano [g,*], Inmaculada López-Aliaga [a,**], Paul D. Cotter [d,e,h], José A. García-Salcedo [b,c,i]

[a] *Department of Physiology (Faculty of Pharmacy, Campus Universitario de Cartuja), Institute of Nutrition and Food Technology "José Mataix Verdú", University of Granada, Granada, Spain*
[b] *GENYO, Centre for Genomics and Oncological Research: Pfizer / University of Granada / Andalusian Regional Government, Granada, Spain*
[c] *Instituto de Investigación Biosanitaria ibs, Granada, Spain*
[d] *VistaMilk SFI Research Centre, Cork, Ireland*
[e] *Teagasc Food Research Centre, Carlow, Ireland*
[f] *Service of Anatomical pathology, Intercenter Regional Unit Granada, University Hospital Virgen de las Nieves, Granada, Spain*
[g] *Center for Intensive Mediterranean Agrosystems and Agri-food Biotechnology (CIAIMBITAL), University of Almeria, Almeria, Spain*
[h] *APC Microbiome Ireland, Cork, Ireland*
[i] *Microbiology Unit, University Hospital Virgen de las Nieves, Granada, Spain*

ARTICLE INFO

Keywords:
Iron deficiency anaemia
Intestinal barrier
Gut microbiome
Microbial translocation

ABSTRACT

Background: Iron deficiency is the top leading cause of anaemia, whose treatment has been shown to deteriorate gut health. However, a comprehensive analysis of the intestinal barrier and the gut microbiome during iron deficiency anemia (IDA) has not been performed to date. This study aims to delve further into the analysis of these two aspects, which will mean a step forward minimising the negative impact of iron supplements on intestinal health.

Methods: IDA was experimentally induced in an animal model. Shotgun sequencing was used to analyse the gut microbiome in the colonic region, while the intestinal barrier was studied through histological analyses, mRNA sequencing (RNA-Seq), qPCR and immunofluorescence assays. Determinations of lipopolysaccharide (LPS) and bacteria-specific immunoglobulins were performed to assess microbial translocation.

Results: Microbial metabolism in the colon shifted towards an increased production of certain amino acids, short chain fatty acids and nucleotides, with *Clostridium* species being enriched during IDA. Structural alterations of the colonic epithelium were shown by histological analysis. RNA-Seq revealed a downregulation of extracellular matrix-associated genes and proteins and an overall underdeveloped epithelium. Increased levels of serum LPS and an increased immune response against dysbiotic bacteria support an impairment in the integrity of the gut barrier during IDA.

Conclusions: IDA negatively impacts the gut microbiome and the intestinal barrier, triggering an increased microbial translocation. This study emphasizes the deterioration of gut health during IDA and the fact that it should be addressed when treating the disease.

Peer review under responsibility of Chang Gung University.

* Corresponding author. Center for Intensive Mediterranean Agrosystems and Agri-food Biotechnology (CIAIMBITAL), University of Almeria, Carretera Sacramento s/nLa Cañada de San Urbano, E-04001, Almería, Andalusia, Spain.

** Corresponding author. Department of Physiology (Faculty of Pharmacy, Campus Universitario de Cartuja), Institute of Nutrition and Food Technology "José Mataix Verdú", University of Granada, Avda. del Hospicio, E-18071, Granada, Spain.

E-mail addresses: msoriano@ual.es (M. Soriano), milopez@ugr.es (I. López-Aliaga).

https://doi.org/10.1016/j.bj.2024.100701
Received 30 May 2023; Received in revised form 9 November 2023; Accepted 19 January 2024
Available online 26 January 2024

1. Background

Anaemia is a public health concern that affects a quarter of the total population, including 47 % of children under 5 years of age and 30 % of pregnant women. Despite being globally distributed, anaemia is over-represented in low-income countries [1], imposing a considerable economic burden.

Iron deficiency is the top leading cause of anaemia [2] and the most common micronutrient deficiency worldwide [3]. Although growing children, pregnant and adult women, and the elderly have been classically considered at risk populations, there is increasing evidence to suggest that iron deficiency anaemia (IDA) can often affect patients suffering a wide variety of disorders, such as inflammatory bowel disease or *Helicobacter pylori* infection [4,5].

The gut microbiome is gaining traction as a target to consider in the pathogenesis of IDA due to its capacity to modulate iron metabolism. Specific microbial metabolites have been shown to impair iron absorption both *in vitro* and *in vivo* through the degradation of hypoxia inducible factor 2 α subunit [6]; others, however, promote iron absorption, such as *p*-hydroxyphenyllactic acid [7].

Iron supplements have been shown to be detrimental to the gut microbiome and the intestinal barrier [8,9], although studies analysing these aspects during IDA are scarce, especially in relation to the gut barrier. There is increasing evidence to suggest that a state of gut dysbiosis exists in the large intestine of patients suffering IDA, with changes in short chain fatty acid (SCFA)-producing genera [10,11], a depletion in the phylum Proteobacteria [12], and a loss of members of the family Ruminococcaceae, order Clostridiales, class Clostridia and the genus *Faecalibacterium* [13]. Altered relative abundances of streptococci were also reported for iron deficient pregnant women [14]. Studies in animals also reveal a gut dysbiosis in the large intestine during IDA [15–17].

The gut microbiome is one of the key components of the intestinal barrier [18]. A wide variety of antigens, toxins and microorganisms are normally found in the intestinal lumen, with the intestinal barrier preventing their leakage into the bloodstream and the consequent disruption of tissue homeostasis. Considerable evidence supports the fact that the loss of integrity in the intestinal barrier along with microbial translocation to extraintestinal sites are involved in the pathogenesis or aggravation of chronic, non-infectious diseases [19]. Iron shortage impairs cell cycle progression and DNA replication [2]. In this sense, intestinal epithelial cells, the mainstay of the intestinal barrier, are characterized by a high turnover rate [18] and are likely to be affected during IDA. Hypoxia inducible factor 1 (HIF1) is also a key regulator of the intestinal barrier. It regulates the expression of genes involved in mucus synthesis, antimicrobial defence, xenobiotic clearance or tight junction proteins [20]. Loss of hypoxia and HIF1 has been related to increased gut permeability [21]. Intestinal hypoxia is maintained via mitochondrial iron-dependent mechanisms involving the bacterial production of SCFAs in the large intestine [22].

Intestinal hypoxia as a component of the gut barrier has not been studied during IDA. In fact, the function of mitochondrial iron-containing cytochromes has been described to be impaired during iron deficiency [23], although its effect on hypoxia levels is largely unknown. Moreover, there are also few studies that investigate the effect of iron deficiency on the intestinal barrier functionality as a whole [24], and none of them provides a comprehensive analysis. Most studies are focused on the implications of iron overload [24,25]. Similarly, existing studies in animal models analysing how the gut microbiome responds to an experimentally induced IDA use 16S rRNA sequencing, which only allows the taxonomic characterisation at the genus level [15–17].

This study aims to address these current gaps in our knowledge providing an in-depth functional and structural characterisation of the colonic microbiome in response to IDA through shotgun sequencing. The intestinal barrier and the extent of microbial translocation will also be analysed and considered within the context of the gut microbiome. Analysing these hallmarks of intestinal health might be important in the clinical management of IDA to take gut protective approaches during the treatment period of the disease, which might contribute to its recovery.

2. Material and methods

2.1. Animal model

Animal housing, care, handling procedures, and experimental protocols were approved by the Ethics Committee of the University of Granada and the local government Junta de Andalucía (ref June 06, 2019/100) in accordance with European guidelines (Declaration of Helsinki; Directive 2010/63/EU). Animal experiments were performed in the Animal Service of the University of Granada, with controlled sanitary and environmental parameters. Twenty weaned male Wistar rats, purchased from Charles River Laboratories (France), were used for the study, with diets and deionized water available *ad libitum*. Animals were housed in groups, using ventilated, thermoregulated cages with controlled temperature (23 ± 2 °C), humidity (60 ± 5 %), and a 12-h circadian rhythm.

IDA was experimentally induced through an iron deficient diet for a period of 40 days, as previously described [26]. Animals were randomly divided into control (n = 11) or anaemic (n = 9) group, receiving the first one the AIN-93G diet [27] and the last one, the iron deficient counterpart. At the end of the experimental period, blood samples were collected from the caudal vein, using EDTA as anticoagulant to control haematological parameters. Animals were then intraperitoneally anesthetized using sodium pentobarbital (Richter Pharma AG, Austria) and bled out by cardiac puncture. Serum samples were obtained from total clotted blood via centrifugation (3000g, 10 min, 4 °C). Colon segments were isolated, contents collected for the study of the gut microbiome and immediately frozen at −80 °C until analysis. The remaining tissue was washed with ice-cold saline solution; one whole slice underwent fixation for immunostaining and histological analysis (see below). The rest was cut open longitudinally and the mucous layer scratched, snap-frozen in liquid nitrogen and stored at −80 °C until analysis. Mucous layer samples were used afterwards for RNA isolation, quantitative PCR (qPCR) and mRNA-sequencing (RNA-Seq).

2.2. Haematological tests

Red blood cell count, haemoglobin concentration, haematocrit, mean corpuscular volume, mean corpuscular haemoglobin, mean corpuscular haemoglobin concentration, leukocyte and platelet count were measured using an automated haematology analyser Mythic 22CT (C2 Diagnostics, France).

2.3. Determination of iron metabolism parameters

Serum iron, total iron binding capacity (TIBC) and ferritin were determined as biomarkers of iron deficiency.

Serum iron and TIBC were determined using the Total Iron-Binding Capacity and Serum Iron Assay Kit (MAK394, Sigma Aldrich, USA), according to the manufacturer's instructions. Ferritin was determined in serum samples via ELISA, using Rat Ferritin ELISA Kit (ab157732, Abcam, UK).

2.4. Shotgun sequencing and bioinformatic analysis

DNA was isolated as described by Soriano-Lerma et al. [15]. Libraries were prepared using the DNA prep protocol (1000000025416, Illumina, USA) with 25–500 ng of input DNA, according to manufacturer's instructions. All samples were quantified using Qubit system 2.0 (Thermo Fisher Scientific, USA) and pooled according to the lowest concentration. Final pool was sequenced using the 2x151 bp P1 reagent (20050264, Illumina, USA) and NextSeq2000 sequencer, obtaining a total of 150 M raw reads.

Quality processing of fastq files was performed using KneadData pipeline. Trimmomatic was used for the quality trimming and Bowtie2 to remove host contaminating sequences belonging to human and rat genomes. Resulting fastq files were converted to fasta using IDBA-UD and processed using HUMAnN 3.0 pipeline [28]. Taxonomy at the species level was assigned via alignment against ChocoPhlAn v30 database and MetaPhlAn classifier. Translated search and functional profiling was performed using DIAMOND aligner and UNIPROT database, clustering sequences at 90% of homology to ensure good representation of gene families in the UniRef clusters; gene families were then regrouped using the Kyoto Encyclopedia of Genes and Genomes (KEGG) orthologs database.

Statistically significant KEGG orthologs (KO) were selected using "edgeR" package and p-adjusted values below 0.05. Selected KOs were then mapped to KEGG pathways, and pathways of interest were coloured according to log2 fold change (log_2FC) values using KEGG Search & Colour pathway tool.

Statistically significant species were determined using ALDEx2 package and p values below 0.05.

2.5. Quantification of bacterial load

To quantify the total bacterial load, 16S rRNA gene-targeted qPCR was performed. Power SYBR green PCR (4309155, Thermo Fisher Scientific, USA) was used in a total reaction mixture volume of 10 µL. The universal bacterial primers were F: 5′-AAACTCAAAKGAATTGACGGGG-3′ and R: 5′-GGGTTGCGCTCGTTRYGG-3' [29]. Primers in a final concentration of 500 nM each and DNA volume of 1 µl (<50 ng) were added to the PCR master mix in MicroAmp Fast 96-Well reaction plates (4346907, Thermo Fisher Scientific, USA). qPCRs were performed using QuantStudio 6 system (Thermo Fisher Scientific, USA) and cycling conditions included 95 °C for 10 min and 40 cycles consisting of denaturalization at 95 °C for 15 s and annealing-extension at 60 °C for 1 min. Negative controls containing no template DNA were subjected to the same procedures. The specificity of the amplified products was determined by analysis of melting curves. The number of 16S copies per sample were obtained via interpolation in the standard curve, for which known concentrations of *Escherichia coli* 16S gene were used.

2.6. SCFAs determination

200 mg of colonic contents were weighed and homogenised in 1.8 mL of saline solution. Suspensions were centrifuged and filtered (0.22 µm) to eliminate suspended particles. Supernatants were transferred to a vial for high performance liquid chromatography (HPLC) analysis using the Acquity UPLC-I Class System (Waters Corporation, USA) with an UV–vis detector set at 210 nm (TUV Detector). Dilutions of SCFAs standards (Acetic acid:A6283, Sigma-Aldrich; Propionic acid: 81,910, Sigma-Aldrich; Butyric acid:108,111,000, Acros Organics) were prepared in saline solution at concentrations ranging from 87 to 0.087 mM for acetic acid, 67–0.067 mM for propionic acid and 54.5–0.0545 mM in the case of butyric acid. A Waters CORTECS™ C18 column (2.1 × 100 mm, 1.6 µm) was used at room temperature, at a flow rate of 0.2 mL/min; water buffer (solvent A)/acetonitrile (solvent B) gradient elution was performed as follows: from 1 to 100% B and down to 1% B, 0–7.5 min. The injected sample volume was 10 uL.

2.7. Histological analysis

Histological analysis was performed as previously described [22], with colon fragments being collected and fixed 8 h (RT) in 4% paraformaldehyde (P6148, Sigma Aldrich, USA). Tissue dehydration, paraffin embedding, sectioning and haematoxylin & eosin staining were performed by Atrys Health S.A (Granada, Spain). Images were obtained using the Olympus BX43 microscope and analysed blindly, calculating histological scores for each parameter as described by Fachi et al. [22].

The Alcian blue staining method was used to specifically dye goblet cells. Briefly, colon fragments were collected and fixed as described earlier (4% paraformaldehyde, 8 h, RT). After sectioning, colon slices were dyed using Alician blue reagent pH 2.5 (101647, Merck) according to the manufacturer's protocol. Quantification was performed using ImageJ and calculating the percentage of area dyed with blue.

2.8. RNA isolation and qPCR

Total cellular RNA was isolated from colonic mucous samples with Trizol Reagent (15596, Invitrogen). Reverse transcription was performed using RevertAid First Strand cDNA Synthesis Kit (K1622, Thermo Fisher Scientific, USA) with Oligo(dT) primers according to the manufacturer's protocol. Quantitative PCR was conducted on QuantStudio 6 (Thermo Fisher Scientific, USA) with SYBR Green (4309155, Thermo Fisher Scientific), a final concentration of primers of 500 nM and using 2 µL of previously diluted cDNA (1:10). Target mRNA levels were normalized in relation to basic transcription factor 3 (BTF3) or anti-cyclophilin B (PPIB). Primers used for this study are listed in [Supplementary Table 1].

2.9. mRNA sequencing (RNA-Seq)

RNA was isolated from colonic mucous layer samples following the already described method (see above). RNA quality was assessed through the determination of the RNA Integrity Number (RIN) via 2100 Bioanalyzer Instrument (Agilent Technologies, USA). mRNA libraries were prepared using 500–1000 ng of total RNA as an input and the polyA selection protocol (TruSeq stranded mRNA Library Prep, ref. 20020595/20020594) at the Centre for Genomic Regulation (Spain). Libraries were then sequenced using the Hiseq2500 platform (Illumina, USA) and the paired-end 50bp format.

A total of 40 million raw reads per sample were obtained and mapped using "Rsubread". Reads were aligned and annotated using the rat genome rn6 as a reference, downloaded from http://hgdownload.soe.ucsc.edu/downloads.html#rat. Further analyses in R software were performed using "edgeR" package. Gene set enrichment analysis (GSEA) was performed using "fgsea" package and log_2FC as the ranking parameter. Gene Ontology (GO) was used as the reference database (including Biological process, Cellular component and Molecular function categories). Differentially expressed GO terms during IDA were selected using p-adjusted values below 0.05; upregulation or downregulation of each pathway was assessed with positive and negative values of the Normalized Enrichment Score (NES), respectively. Visualization of parental terms was performed using REVIGO tool [30]; results derived from GSEA were also plotted using GOplot package [31].

2.10. Immunofluorescence

Colon fragments were harvested, washed and fixed 8 h (RT) in 4% paraformaldehyde (P6148, Sigma Aldrich, USA). Tissues were embedded in Tissue-Tek OCT Compound (Sakura Finetek, USA), frozen using isopentane and dry ice and stored at −80 °C. Sections were cut (4 µm) using a cryostat and labelled overnight at 4 °C with COL6 antibody (1:500) (MA5-32412, Thermo Fisher Scientific, USA) or the mitosis marker phospho-histone 3 serin 10 (pH3S10) [32] (1:500, 2 h, RT) (ab47297. Abcam). Then, nonspecific binding sites were blocked with 10% bovine serum albumin (A7906, Sigma Aldrich, USA), 0.5% (v/v) Triton-X100 for 30 min. A secondary antibody conjugated with AlexaFluor-555 (A-31572, Thermo Fisher Scientific, USA) was used for detection (1:1000). Counterstaining was performed using DAPI (0.5 µg/mL) (Invitrogen, USA). Sections were mounted in Vectashield medium (Vector Laboratories, USA). Images were acquired through a Confocal Zeiss LSM 710 inverted microscope. Immunofluorescence images were quantified measuring the area positive for both DAPI and antibody signal using ImageJ. To allow comparability, instrument

settings were equally adjusted across samples.

2.11. Detection of bacteria-specific IgG, IgM and IgA

The determination of faecal bacteria-specific immunoglobulins was performed via ELISA as previously described [33]. Faecal bacteria belonging to the anaemic or control group were obtained using 200 mg of faecal pellets. After homogenization in sterile PBS, filtration through a 100 µm strainer, bacteria were separated from debris/rat cells by removing the pellet after centrifugation at 400 *g* for 10 min (4 °C). Faecal bacteria were washed, heat-killed at 85 °C for 1 h, and resuspended in 20 mL PBS, and 100 µL of this suspension was added to each well of a 96-well ELISA plate for overnight coating at 4 °C. Number of bacteria in each suspension was determined by spectrophotometry at 600 nm and adjusted across experimental groups. Wells were then blocked with 1% (w/v) BSA in PBS for 2 h at room temperature. Rat sera were diluted at 1:100 and incubated overnight at 4 °C for detection of IgG, IgM, and IgA. Incubation with secondary anti-rat IgG, IgM and IgA antibodies (A110-143P, BioNova científica S.L., Spain) (1:10000) for 1.5 h in darkness was followed by the addition of HRP substrate (11112422001, Roche Applied Science, Germany). Absorbance was measured using NanoQuant Infinite M200 Pro multi-plate reader (Tecan, Switzerland).

2.12. Lypopolysaccharide (LPS) detection

LPS determination was performed using LAL chromogenic assay (A39552, Thermo Fisher Scientific, USA), according to manufacturer's instructions. Serum samples were diluted 1:20 and heat inactivated at 70 °C for 15 min.

2.13. Statistical analysis

Pearson correlations between SCFAs and statistically significant species were calculated using R software. Network diagrams were plotted using Gephi 0.9.2.

Statistical analysis was performed using Prism GraphPad software, or R software in case of RNA-Seq and shotgun experiments. Statistical significance was assessed using Student's two-tailed *t*-test or a non-parametric alternative in case data were not normally distributed. In RNA-Seq and shotgun analysis, p-adjusted values were used to determine differentially expressed GO terms or statistically significant KO genes.

For all tests, p values below 0.05 were considered significant (unless otherwise indicated) and expressed as follows: $*p < 0.05$, $**p < 0.01$, $***p < 0.001$ and $****p < 0.0001$.

3. Results

3.1. Determination of haematological parameters and study of iron metabolism confirmed the induction of IDA

A decrease in the number of red blood cells, haemoglobin concentration, haematocrit, mean corpuscular volume and mean corpuscular haemoglobin concentration by day 40 (d40) confirmed that IDA had been correctly induced [Table 1].

A decrease in serum iron and ferritin along with an increase in TIBC also confirmed iron deficiency in the anaemic animals [Table 2]

3.2. Microbial metabolism and gut microbiome structure shifted in response to IDA

Having previously provided a comprehensive view of gut microbial alterations occurring during IDA along the gastrointestinal tract [15], the colon was identified as the region showing the greatest dysbiosis and its microbiome was characterized using shotgun sequencing.

Table 1
Haematological parameters during the development of iron deficiency anaemia (day 40).

Haematological parameter	Control (n = 11)	Anaemia (n = 9)
	Day 40	Day 40
Red blood cells (10^6/µL)	8.12 ± 0.45	2.15 ± 0.51*
Haemoglobin (g/dL)	16.05 ± 0.89	4.16 ± 0.52***
Haematocrit (%)	47.89 ± 2.75	21.34 ± 9.27***
Mean corpuscular volume (fL)	59.14 ± 1.54	40.22 ± 0.65***
Mean corpuscular haemoglobin (pg)	19.82 ± 0.67	20.60 ± 6.27
Mean corpuscular haemoglobin concentration (g/dL)	33.49 ± 0.75	25.95 ± 17.11**
Leukocytes (10^3/µl)	13.23 ± 2.25	10.51 ± 1.48
Platelets (10^3/µL)	889.64 ± 445.55	Over range

Means and standard deviations are shown for each group and parameter. Statistical significance is expressed as follows: $*p < 0.05$, $**p < 0.01$ and $***p < 0.001$.

Table 2
Study of iron metabolism.

Parameters	Control (n = 10)	Anaemia (n = 8)
	Day 40	Day 40
Serum iron (µg/L)	1293 ± 80.12	613 ± 43.98***
TIBC (µg/L)	2740 ± 189	18110 ± 570***
Ferritin (µg/L)	81.5 ± 2.6	48.3 ± 2.01***

Abbreviations: TIBC: total iron binding capacity. Means and standard deviations are shown for each group and parameter. Statistical significance is expressed as follows: $*p < 0.05$, $**p < 0.01$ and $***p < 0.001$.

A total of 142 M reads were obtained after bioinformatic processing. To analyse the microbial functional traits, differentially abundant KO genes between the control and anaemic groups were determined [Supplementary Fig. 1 [Supplementary Table 2]; most genes showed positive values of $\log_2$FC indicating a higher abundance during IDA [Supplementary Fig. 1]. To assess whether these bacterial genes clustered specifically in pathways, differentially abundant KOs were selected and mapped onto KEGG pathways [Fig. 1]. Additional information on mapped KOs is displayed in [Supplementary Table 3].

Pathways of interest were then coloured according to $\log_2$FC values of differentially abundant KO genes, revealing a general increased abundance of genes related to biosynthesis of amino acids [Supplementary Fig. 2], amino sugar and nucleotide metabolism [Supplementary Fig. 3], glyclolysis and gluconeogenesis [Supplementary Fig. 4], pyruvate metabolism [Supplementary Fig. 5], butanoate metabolism [Fig. 2], propanoate metabolism [Fig. 3], purine metabolism [Supplementary Fig. 6] and pyrimidine metabolism [Supplementary Fig. 7] during IDA.

KO genes involved in the synthesis of certain amino acids were more abundant during IDA, such as tyrosine, phenylalanine, cysteine, methionine or alanine ([Supplementary Fig. 2], final products highlighted in green squares), while KOs involved in the synthesis of valine, leucine, or isoleucine were decreased ([Supplementary Fig. 2], final products highlighted in orange squares).

Analysis of amino sugar and nucleotide metabolism revealed a higher abundance of genes associated with peptidoglycan production ([Supplementary Fig. 3], pathway steps highlighted in green arrows) and with the synthesis of metabolic sugar intermediates, such as Glucose-6-P, Fructose-6-P or Mannose-6-P ([Supplementary Fig. 3], pathway steps highlighted in blue arrows). As far as glycolysis and gluconeogenesis is concerned, KO genes related to the transformation of monosaccharides and sugar intermediates, such as the above-mentioned ones, into pyruvate and acetyl-CoA were enriched in anaemic animals

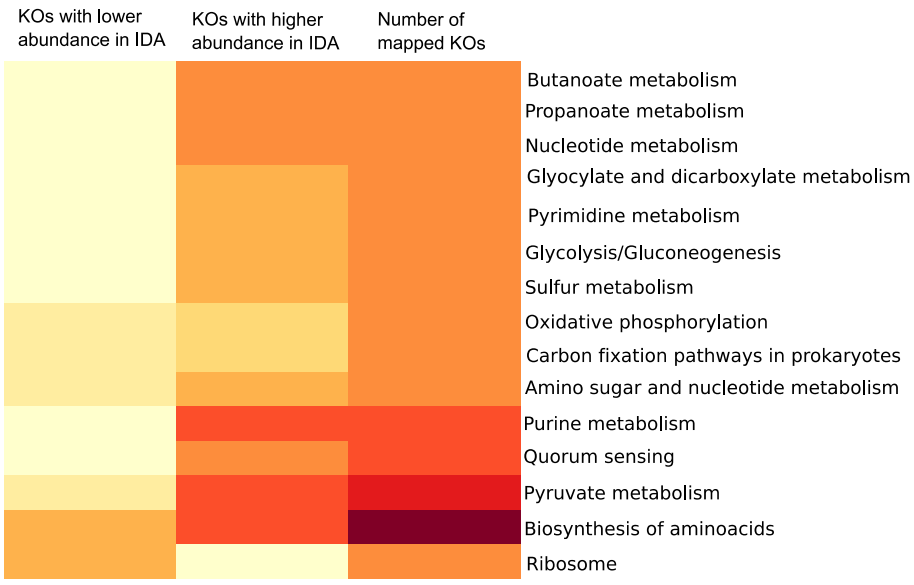

Fig. 1. Heatmap showing statistically significant KOs mapped onto KEGG pathways; redder colours indicate higher numbers. Only pathways containing between 50 and 20 mapped KOs were considered to exclude the most general and the least abundant ones.

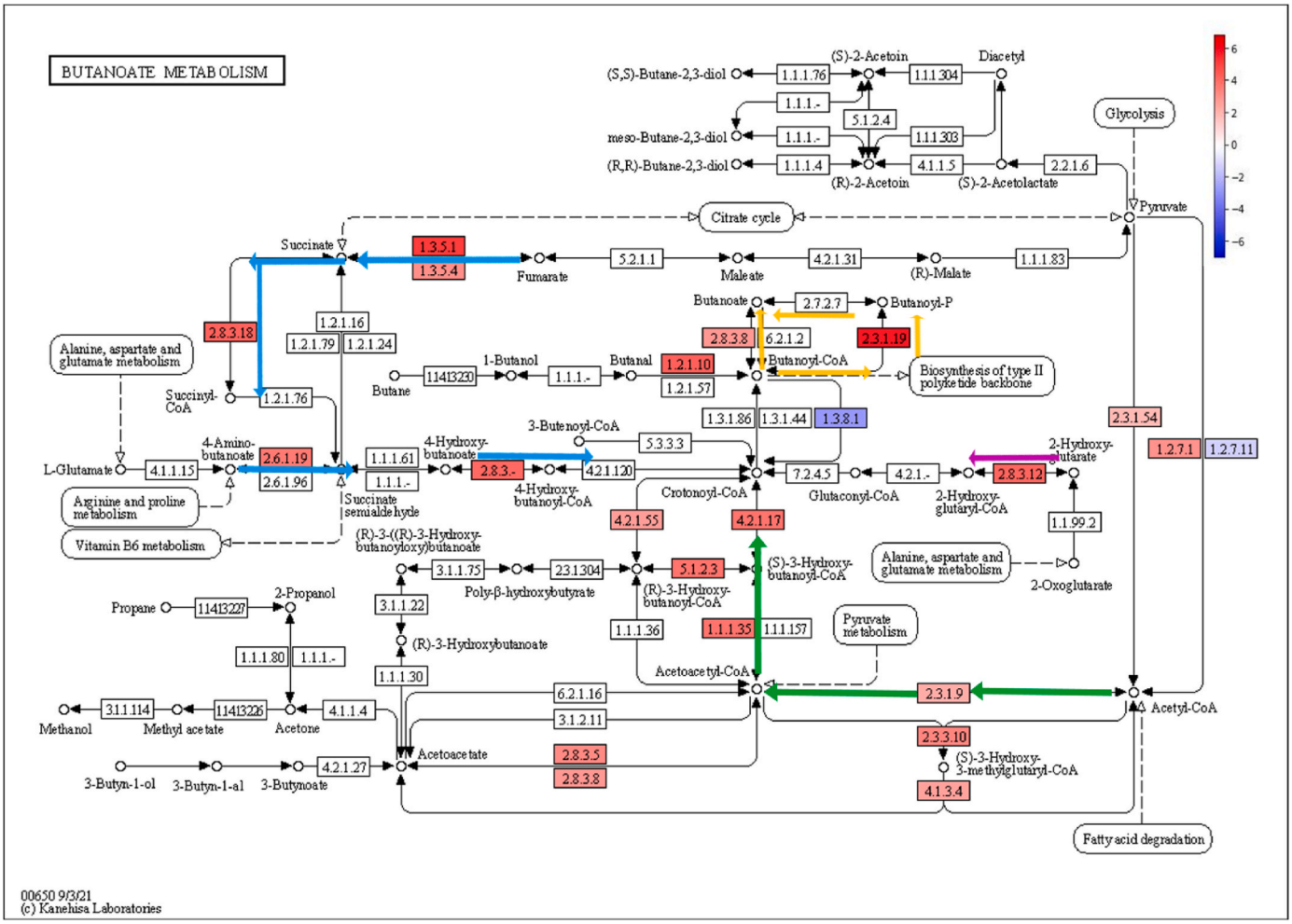

Fig. 2. Butanoate metabolism pathway (KEGG) coloured according to $\log_2$FC values of statistically significant KO genes. Colour legend: KO genes with increased relative abundance during IDA (red); KO genes with decreased relative abundance during IDA (blue); 4-aminobutanoate/succinate pathway (blue), Acetyl-CoA pathway (green), glutarate pathway (pink), Butanoyl-CoA – Butanoate conversion (orange).

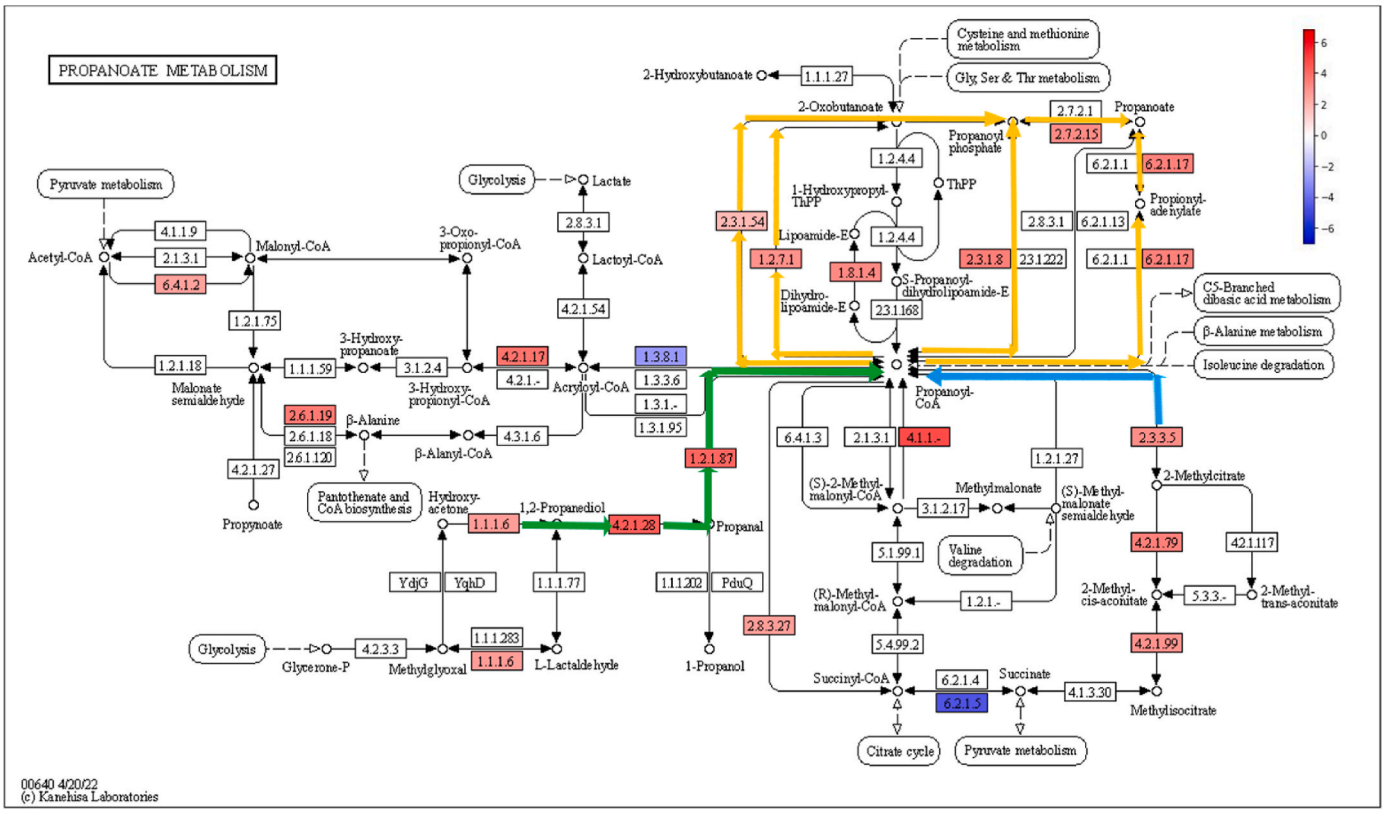

Fig. 3. Propanoate metabolism pathway (KEGG) coloured according to $\log_2$FC values of statistically significant KO genes. Colour legend: KO genes with increased relative abundance during IDA (red); KO genes with decreased relative abundance during IDA (blue); 1,2-propanediol pathway (green), 2-methylcitrate pathway (blue), Propanoyl-CoA – Propanoate conversion (orange).

([Supplementary Fig. 4], pathway steps highlighted in blue arrows). KO genes involved in the metabolism of pyruvate showed also increased abundances during IDA, leading to the formation of formate, succinate ([Supplementary Fig. 5], pathway steps highlighted in blue arrows) and lactate and acetate ([Supplementary Fig. 5], pathway steps highlighted in green arrows). Most KO genes belonging to the acetyl-CoA and 4-aminobutanoate/succinate pathway were increased within the butanoate metabolism during IDA ([Fig. 2], pathway steps highlighted in green and blue arrows respectively). Similarly, part of the glutarate pathway also showed higher abundance ([Fig. 2], pathway steps highlighted in pink arrows), as well as last steps involving the transformation of butanoyl-CoA into butanoate ([Fig. 2, pathway steps highlighted in orange arrows). In the case of propanoate metabolism, most pathways involved in the transformation of propanoyl-CoA into propanoate were more abundant in the anaemic group ([Fig. 3], highlighted in orange), along with the 1,2-propanediol pathway ([Fig. 3], pathway steps highlighted in green arrows) and the 2-methylcitrate pathway ([Fig. 3], pathway steps highlighted in blue arrows). Determination of butanoate, propanoate and acetate in the colon of control and anaemic animals confirmed an increased production of SCFAs during IDA [Supplementary Fig. 8].

Lastly, purine and pyrimidine pathways were characterized by an increased abundance of genes related to the production of guanine, xanthine, hypoxanthine and adenine in the case of purine metabolism ([Supplementary Fig. 6], pathway steps highlighted in green arrows), and uracil, cytosine and thymine in the case of pyrimidine metabolism ([Supplementary Fig. 7], pathway steps highlighted in green arrows). KO genes involved in the production cyclic AMP and GMP, along with hyperphosphorylated guanine derivatives (pppGpp and ppGpp), were also more abundant during IDA ([Supplementary Fig. 6], pathway steps highlighted in pink arrows).

Since high synthesis of nucleotides suggest a high division rate, bacterial load was quantified by qPCR in colonic content samples belonging to anaemic and control animals. A higher number of 16S rRNA copies was found during IDA [Supplementary Fig. 9].

Analysis of the differentially abundant bacterial taxa showed that *Clostridium* species, among others, were more abundant during IDA [Fig. 4A]. Since members of the genus *Clostridium* are among the major producers of SCFAs in the large intestine [34], Pearson correlations were calculated between SCFAs and differentially abundant species and plotted in a network diagram [Fig. 4B]. Node size was adjusted according to their connectivity, and so was colour using a blue-to-red scale. Correlations were plotted as edges using the same colour scale, with blue and red edges indicating negative and positive correlations, respectively. All *Clostridium* species (*Clostridium simbiosum*, *Clostridium disporicum*, *Clostridium perfringens, Clostridium innocuum* and *Clostridium bolteae*) showed positive correlations to butanoate and propanoate, and negative correlations to acetate.

3.3. *Changes in colonic metabolism during IDA reveals hypoxia-independent alterations in the intestinal barrier*

First, histological analysis was performed to provide a comprehensive view of the integrity of the colonic epithelium. Considerable epithelial damage and ulceration was found during IDA, along with leukocyte infiltration into the lamina propia and submucosa ([Supplementary Fig. 10A], red and black arrows respectively). A depletion of goblet cells was also noticed in anaemic animals ([Supplementary Fig. 10A], asterisks). Histological scores, indicating an altered structure of the epithelium, were calculated for both groups, with increased values in the anaemic group [Supplementary Fig. 10B]. Alcian blue staining confirmed goblet cells were depleted during IDA [Supplementary Fig. 11]. Mitosis was evaluated via immunofluorescence using the pH3S10 antibody in colon sections, revealing cells

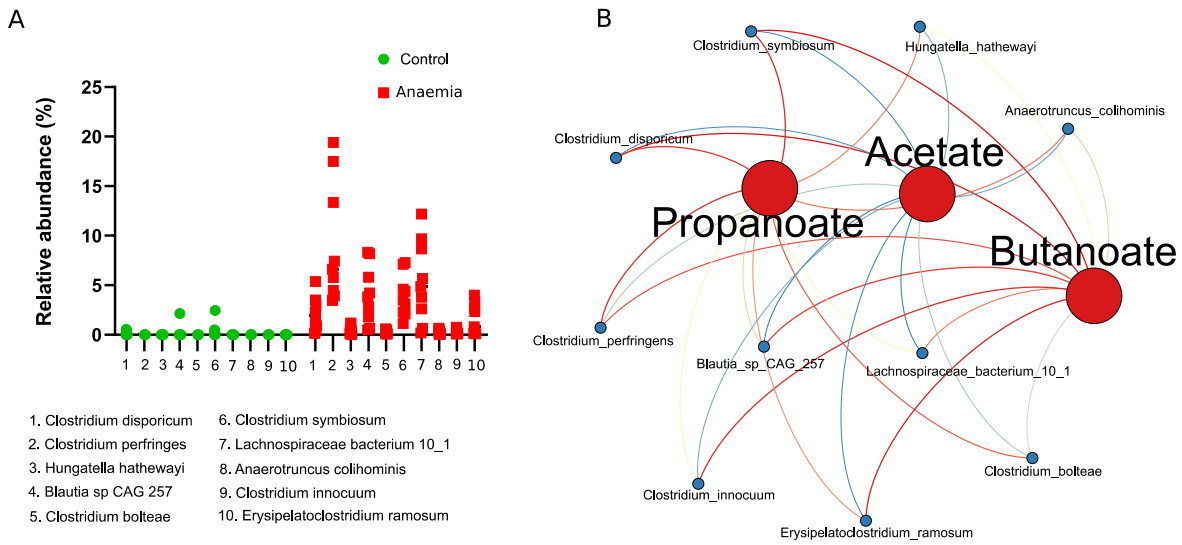

Fig. 4. Taxonomic analysis at the species level and Pearson correlations between statistically significant species and SCFAs levels. (A) Scatter plot of differentially abundant species ($p < 0.05$) in the control and anaemic group determined by ALDEx2 (B) Network diagram illustrating Pearson correlations between species in A and SCFAs levels. Node size and colour have been adjusted according to its connectivity in a blue-to-red scale; edges have been coloured using the same scale, whereby blue and red indicate negative and positive correlations.

undergoing mitosis were diminished during IDA [Supplementary Fig. 12].

RNA-Seq was performed to gain insight into alterations in gene expression taking place during IDA in the colonic epithelium.

Gene set enrichment analysis (GSEA) was next applied to assess whether deregulated genes during anaemia clustered in specific Gene Ontology (GO) terms [Supplementary Table 4]. GO database was used including all categories (Biological process, Cellular component and Molecular function). Significant parental terms resulting from GSEA were divided into upregulated (Normalized Enrichment Score, NES >0) [Fig. 5A, C, 5E] or downregulated pathways (NES <0) [Fig. 5B, D, 5F] for each category, and represented in a bubble plot. Each bubble represents a significantly deregulated parental GO term, grouped by semantic similarity. The colour of the bubbles is indicative of the NES value; the brighter the blue, the higher absolute value of NES, which indicates that particular GO term is strongly deregulated. Bubble size is indicative of how general the GO term is in the Gene Ontology Annotation database; larger sizes indicate more general terms with higher number of child terms. Only the most representative GO terms (larger sizes, see legend) were displayed to facilitate visualization.

Downregulated GO terms outnumbered upregulated ones. It is notable the fact that upregulated GO terms included those involved in lipid metabolism (highlighted in blue), metabolic pathways in response to microorganisms (highlighted in red) and mitochondria-related pathways (highlighted in yellow). On the contrary, GO terms related to the development of the enteric nervous system and the digestive tract (highlighted in black) were downregulated, along with those involved in the neural signalling within the enteric nervous system (highlighted in green). Cell junction assembly and cell integrity GO terms (highlighted in orange), along with extracellular matrix-associated ones (highlighted in pink) were also downregulated.

To analyse individual gene deregulation and the extracellular matrix as a key component of the intestinal barrier [35,36], some GO terms related to collagen metabolism were represented in a chord diagram, along with GO terms associated with colonic intestinal dysbiosis and SCFAs (lipid) metabolism during IDA. On the left part, genes and their corresponding $\log_2$FC are associated to one or more selected GO terms, shown on the right [Fig. 6]. Downregulated genes belonged to extracellular matrix-associated pathways while upregulated ones belonged to GO terms involved in host-microbial interactions and lipid metabolism [Fig. 6]. Interestingly, a considerable number of genes relating to the collagen family of proteins were downregulated. Namely, *Adipocyte enhancer binding protein 1* (*AEBP1*), *collagen VI alpha 1 chain* (*COL6A1*), *fibronectin 1* (*FN1*), *lumican* (*LUM*) and *fibroblast growth factor 13* (*FGF13*) (highlighted in red) were selected along the whole spectrum of downregulation to be validated by quantitative PCR (qPCR) [Fig. 7A]. *COL6A1* was the most significantly downregulated gene during IDA [Fig. 7A], and COL6 protein levels were assessed via immunofluorescence [Fig. 7B], finding also a significant decrease [Fig. 7C].

Given the importance of HIF1α in the maintenance of the intestinal barrier and its dependence on SCFAs levels and mitochondrial iron containing complexes, HIF1α target genes were also studied by qPCR during IDA in the colonic epithelium.

Specific HIF1α targets related to the intestinal barrier were selected, namely *5′-nucleotidase ecto* (*NT5E*), *ectonucleoside triphosphate diphosphohydrolase 1* (*ENTPD1*), *claudin 1* (*CLD1*), *multidrug resistance 1 gene* (*MDR1*) and *mucin 2* (*MUC2*) [20,37,38], and their expression measured in the colonic mucous of anaemic and control animals. Surprisingly, no significant changes were observed in any gene between experimental groups [Supplementary Fig. 13].

3.4. *Increased LPS translocation and immune response towards dysbiotic bacteria is observed during IDA as a consequence of the impaired gut barrier*

LPS translocation was analysed in serum samples, along with bacteria-specific immunoglobulins, to assess the consequences of the impaired gut barrier.

LPS detection in serum samples was significantly higher for anaemic rats compared to control ones [Fig. 8A]. When assessing immune response, immunoglobulin detection against autologous faecal bacteria was greater for anaemic animals compared to control ones [Fig. 8B], “Paired faeces”). However, no significant differences were found in the heterologous immune response of the control and anaemic animals against bacteria obtained from faeces belonging to the control group ([Fig. 8B], “Control faeces”).

4. Discussion

Complex interactions take place between the host and the gut

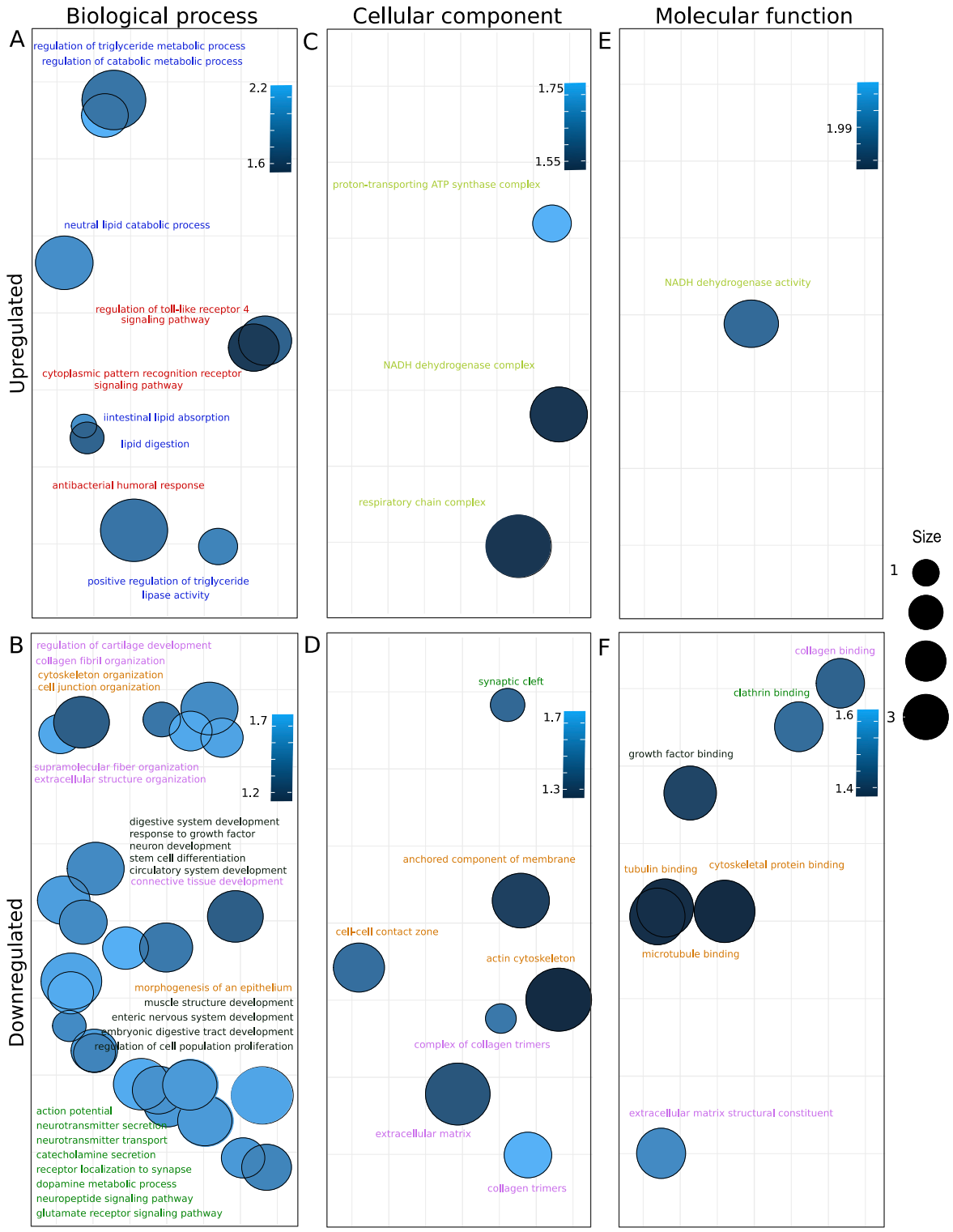

Fig. 5. Bubble plots representing parental upregulated (Normalized Enriched Score, NES>0) or downregulated (NES<0) GO terms grouped by semantic similarity (REVIGO tool) [30]; the X and Y axes represent semantic spaces. Bubble colour have been adjusted according to NES values: the brighter the blue, the higher absolute value of NES and greater deregulation. Bubble size is indicative of how general the GO term is in the Gene Ontology Annotation database; larger sizes indicate more general terms with higher number of child terms. Only the most general GO terms were displayed to facilitate visualization. A and B represents Biological process category, C and D Cellular component category and E and F Molecular Function category. (A) Upregulated parental GO terms during IDA (Biological process category). (B) Downregulated parental GO terms during IDA (Biological process category). (C) Upregulated parental GO terms during IDA (Cellular component category). (D) Downregulated parental GO terms during IDA (Cellular component category). (E) Upregulated parental GO terms during IDA (Molecular function category). (F) Downregulated parental GO terms during IDA (Molecular function category). Colour legend: blue (lipid metabolism); red (host-microbe interactions); yellow (mitochondrial related pathways); orange (cell junction, integrity, cytoskeletal organization); green (synaptic signalling); black (development of enteric nervous system and digestive tract); pink (extracellular matrix).

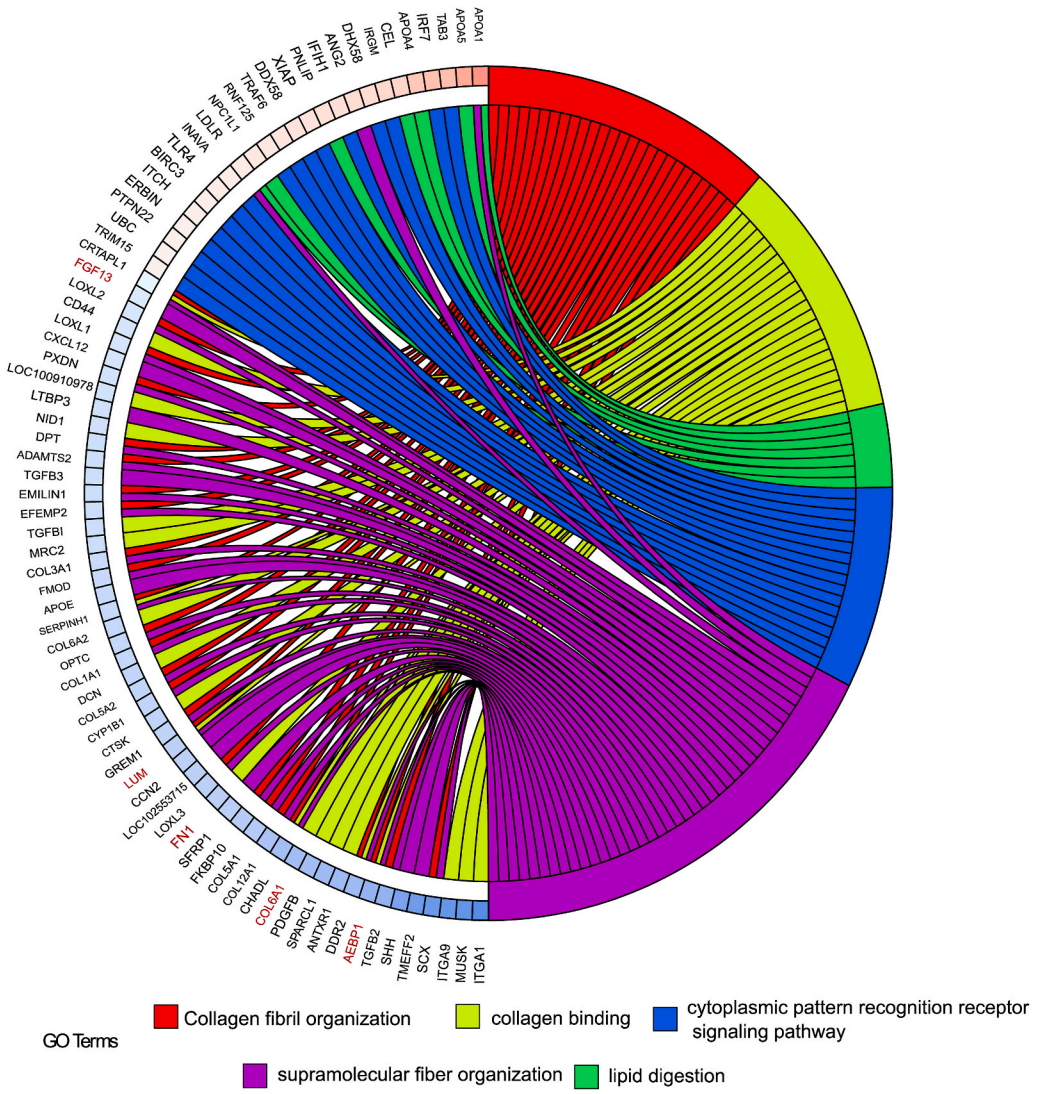

Fig. 6. Identification of key altered genes in the colonic mucous during IDA. Chord diagram illustrating the relationships between the list of selected GO terms and their leading-edge subset of genes obtained from GSEA, including $\log_2$FC values. Left half of the chord diagram displays whether genes are up- or downregulated during IDA; genes are linked to one or several GO terms (right half) by coloured bands, according to the legend. Highlighted in red are the selected genes for qPCR validation.

microbiome, especially when the state of health is compromised. This study aims to provide an in-depth insight into the gut microbiome in the most affected intestinal region during IDA through shotgun sequencing. A comprehensive analysis of the transcriptional changes occurring in the colonic epithelium was also carried out, including a structural analysis of the intestinal barrier and the study of intestinal barrier biomarkers such as extracellular matrix associated genes and proteins and HIF1α target genes. Lastly, microbial translocation was assessed as an indicator of the barrier permeability.

According to Malinowska et al. [39], diet is a key influential factor on the gut microbiome functioning. During iron deficiency, metabolism of carbohydrates leaned towards an increased processing of monosaccharides through the amino sugar and nucleotide pathway ([Supplementary Fig. 3], highlighted in green and blue, respectively), glycolysis and gluconeogenesis ([Supplementary Fig. 4] and pyruvate metabolism [Supplementary Fig. 5]). End products included acetyl-CoA, formate, lactate or succinate. According to Koh et al. [40],lactate and succinate are mainly used as intermediates for the production of SCFA. In fact, the acetyl-CoA and 4-aminobutanoate/succinate pathways within butanoate metabolism were increased during IDA [Fig. 2, highlighted in green and blue respectively]. Similarly, certain amino acids, such as cysteine, methionine and alanine, whose synthesis pathways were increased during IDA ([Supplementary Fig. 2], highlighted in green squares), can also be utilized in the production of SCFAs [41]. Genes related to the synthesis of branched chain amino acids (BCAA) valine, leucine and isoleucine were decreased ([Supplementary Fig. 2], highlighted in orange squares). This is in accordance with the observed levels of SCFA, as BCAA are used to synthesize branched SCFA (valerate, isovalerate and isobutyrate) over SCFA [40].

Moreover, microbial metabolism in the colon shifted towards an increased production of nucleotides and nucleotide derivatives ([Supplementary Fig. 6], highlighted in green and pink, respectively; [Supplementary Fig. 7], highlighted in green), which is indicative of a higher division rate [Supplementary Fig. 9]. Metabolic intermediates such as Glucose-6-P or Fructose-6-P [Supplementary Figs. 3 and 4] are involved in the pentose phosphate pathway, whose main function is to provide NADPH and ribose-5-P for nucleic acid synthesis [42]. Synthesis of hyperphosphorylated guanine derivatives have been related to cellular reprogramming occurring during stress in bacteria [43], such as iron-limiting conditions. These molecules, as well as cyclic nucleotides, can also be involved in quorum sensing signalling, regulating bacterial communication with the environment [44]. Lastly, purine metabolism

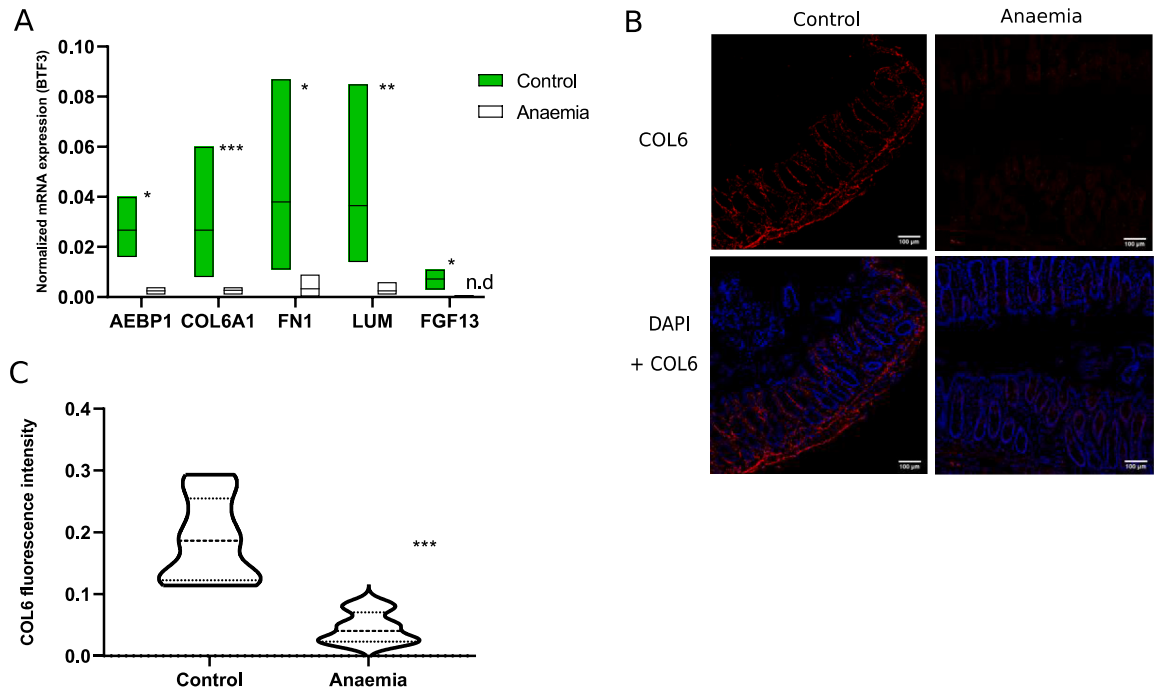

Fig. 7. Validation of genes and proteins selected from RNA-Seq. (A) qPCR validation of previously selected genes. Normalized mRNA expression was calculated using BTF3 as housekeeping gene. *, ** or *** indicate the level of statistical significance between experimental groups. n.d.: not detected (B) Immunofluorescence showing COL6 staining (red) in colonic mucous slides belonging to anaemic and control animals; counterstaining was performed using DAPI (blue) (C) Quantification of COL6 fluorescence levels from sections in (B) by Image J (n = 10 images per experimental group).

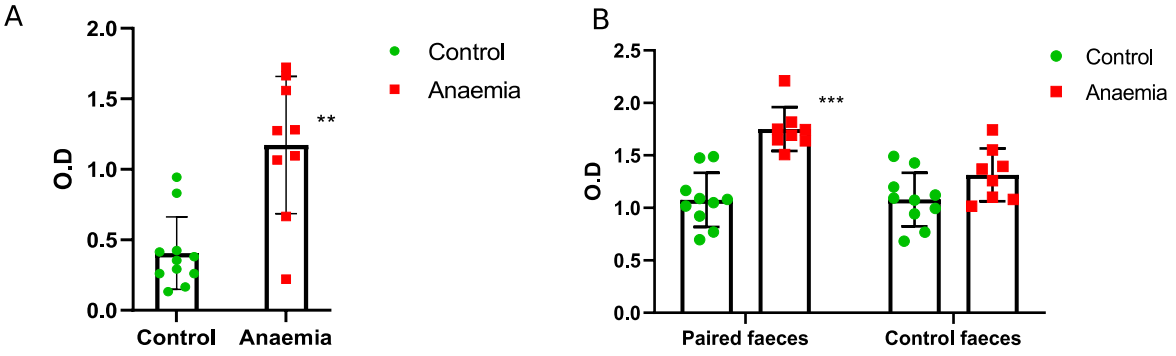

Fig. 8. Study of microbial translocation biomarkers in serum samples belonging to anaemic and control animals. Mean and standard deviations, along with individual values for each sample (green circles for the control group and red squares for the anaemic group) are shown for biological replicates. Statistical significance is expressed as follows: *$p < 0.05$; **$p < 0.01$ and ***$p < 0.001$ (A) LPS levels in both experimental groups. (B) Bacteria-specific IgG, IgA and IgM in serum samples of both experimental groups. Left bar diagram shows the autologous immune response of control and anaemic animals against bacteria obtained from faecal pellets belonging to their own experimental group (*Paired faeces*). Right bar diagram represents the heterologous immune response of control and anaemic animals against bacteria obtained from faecal pellets belonging to the control group (*Control faeces*).

and regulation of the ATP/adenosine pool has been shown to contribute to protecting the intestinal epithelium against intestinal injury [45].

In accordance with Cheng et al. [46], structural alterations of the colonic epithelium were observed during IDA, including epithelial damage and leukocyte infiltration into the lamina propia and submucosa [Supplementary Fig. 10A]. Depletion of goblet cells was also observed during IDA [Supplementary Fig. 11] as well as a reduction in the number of cells undergoing mitosis [Supplementary Fig. 12]. mRNA isolated from colonic mucous samples was sequenced in an attempt to identify the most important changes at the transcriptional level and relate them to the gut microbiome structure and functioning and the intestinal barrier. The gut barrier is considerably affected during IDA, and our results suggest the gut microbiome might be exerting trade-off effects through the production of SCFAs. In fact, GO terms related to lipid metabolism and host-microbial interactions are upregulated in the colonic epithelium, suggesting a crosstalk occurring between the host and the microbiome mediated by SCFA ([Fig. 5A], highlighted in blue and red respectively,[Fig. 6])

GSEA revealed a general downregulation during IDA [Fig. 5B, 5D, and 5F], which is indicative of an impaired gut barrier. Among others, the development of the digestive system and the enteric nervous system was negatively affected during IDA [Fig. 5B]. Iron shortage can impair cell cycle progression [2], causing an underdeveloped intestinal epithelium, and some authors have proposed glial cells as modulators of barrier permeability [19]. In this sense, SCFAs might be involved in increasing enteric neural survival and neurogenesis [47] as well as in promoting natural turnover of colonocytes to make up for an underdeveloped epithelium [40]. However, excess of SCFA could lead to an

accumulation inside cells and apoptosis or a diminished immune response against leaking microorganisms [40].

Importantly, extracellular matrix-associated pathways and genes were also diminished during IDA ([Fig. 5B, 5D, and 5F] highlighted in pink, [Figs. 6 and 7]). Extracellular matrices are three-dimensional networks mainly composed of collagens and other macromolecules. Not only do they provide a physical scaffold for the development of tissues and organs but they also supply cells with chemicals to regulate proliferation, survival and differentiation [48]. Disruption of the extracellular matrix has been related to damage in the intestinal barrier, while its recovery has been associated with the restoration of the intestinal epithelium [35,36]. Iron containing proteins are required for collagen metabolism [49], which supports the downregulation of collagen genes during IDA [Fig. 6]. In particular, *COL6A1* mRNA and COL6 protein levels were validated by qPCR and immunofluorescence, confirming a decrease in the colonic mucous of anaemic animals [Fig. 7A, B and 7C].

Surprisingly, no differences in HIF1α targets were found between the anaemic and control groups [Supplementary Fig. 13] despite the increase in SCFA [Supplementary Fig. 8] and the upregulation of GO terms related to the mitochondrial respiratory chain [Fig. 5C], both involved in HIF1α stabilisation [50]. Decrease in HIF1α might have occurred at earlier timepoints as a consequence of a dysfunctional mitochondrial electron transport chain due to iron deficiency. We hypothesize that the increase in SCFA and the upregulation of mitochondrial pathways are contributing to the maintenance of HIF1α levels and derived gut barrier functions in the colonic epithelium. A normoxic environment derived from loss of hypoxia would be detrimental to the gut microbiome since most microorganisms are anaerobic to some extent [51]; hence, microbial responses are triggered to preserve hypoxia and protect their biological niche. Altogether, these results suggest that the observed damage in the intestinal barrier is independent of hypoxia levels.

Lastly, LPS and bacteria-recognizing Ig were measured in serum samples to assess whether the impaired barrier functionality was responsible for an increased translocation during IDA. LPS levels were increased in serum samples belonging to anaemic animals compared to control ones [Fig. 8A]. Immunoglobulin detection of autologous faecal bacteria was also higher for the anaemic group, while no differences between anaemic and control animals were found when assessing immune response towards bacteria obtained from faecal control samples [Fig. 8B]. These results suggest an increased immune response is occurring against dysbiotic gut bacteria during IDA. Even though SCFAs production seems to play a beneficial role in this context, intestinal dysbiosis is known to trigger inflammatory and immune responses [19].

5. Conclusions

The results presented in this study show that IDA has a considerable impact on the gut microbiome, colonic metabolism and the intestinal barrier. An alteration in the structure of colonic microbial communities occurred in response to IDA, with a predominance of *Clostridium* species, high production of SCFAs and increased bacterial load. An overall deteriorated state of the colonic epithelium was also found, with structural components of the gut barrier being affected by iron deficiency, such as extracellular matrix-associated genes and proteins. As a result, increased levels of LPS were found in serum samples of anaemic animals along with an increased immune response towards gut dysbiotic bacteria. Further investigation is still needed with regards to the effects of SCFAs and the implication of hypoxia as a modulator of the gut barrier functionality during IDA. The existing intestinal dysbiosis and the intestinal barrier functionality should be restored during the treatment period of IDA and might even lead to a more efficient recovery of the disease.

Ethics approval

Animal housing, care, handling procedures, and experimental protocols were approved by the Ethics Committee of the University of Granada and the local government Junta de Andalucía (ref June 06, 2019/100) in accordance with European guidelines (Declaration of Helsinki; Directive 2010/63/EU).

Data availability statement

All datasets supporting the conclusions of this article will be available at the Sequence Read Archive (SRA) of the National Centre for Biotechnology Information (NCBI) upon request. Authors can confirm that all relevant data are included in the article and/or its supplementary information files.

Funding

This work was financially supported by the local government Junta de Andalucía through PAIDI research groups (BIO344 and AGR206), the Ministry of Science and Innovation of Spain (Ref: PID2020-120481RB-I00/AEI/10.13039/501100011033), the University of Almería (Ref: PPUENTE2021-006), Health Instute Carlos III (Acción Estratégica en Salud, PI21/00497), the University of Granada (PPJIB2020-02) and the European Molecular Biology Organization (short stay fellowships program, ref 8626). A.S.L. was supported by a fellowship from the Ministry of Education, Culture and Sport (FPU 17/05413). M.G.B. was financially supported by the program CONTRATOS PUENTE from the University of Granada.

Declaration of competing interest

The authors declare that they have no competing interests.

Acknowledgements

The authors would like to thank Dr Fiona Crispie, Teagasc Agriculture and Food Development Authority (Ireland) and the Genomics Unit at the Center for Genomic Regulation (Spain) for their assistance in the sequencing service. The authors are grateful to Atrys Health S.A (Granada, Spain) for their assistance in the histological analysis.

Appendix A. Supplementary data

Supplementary data to this article can be found online at https://doi.org/10.1016/j.bj.2024.100701.

References

[1] Balarajan Y, Ramakrishnan U, Ozaltin E, Shankar AH, Subramanian SV. Anaemia in low-income and middle-income countries. Lancet 2011;378(9809):2123–35.
[2] Cappellini MD, Musallam KM, Taher AT. Iron deficiency anaemia revisited. J Intern Med 2020;287(2):153–70.
[3] Percy L, Mansour D, Fraser I. Iron deficiency and iron deficiency anaemia in women. Best Pract Res Clin Obstet Gynaecol 2017;40:55–67.
[4] Ghishan FK, Kiela PR. Vitamins and minerals in inflammatory bowel disease. Gastroenterol Clin North Am 2017;46(4):797–808.
[5] Stein J, Connor S, Virgin G, Ong DE, Pereyra L. Anemia and iron deficiency in gastrointestinal and liver conditions. World J Gastroenterol 2016;22(35):7908–25.
[6] Das NK, Schwartz AJ, Barthel G, Inohara N, Liu Q, Sankar A, et al. Microbial metabolite signaling is required for systemic iron homeostasis. Cell Metab 2020;31(1):115–30.
[7] González A, Gálvez N, Martín J, Reyes F, Pérez-Victoria I, Dominguez-Vera JM. Identification of the key excreted molecule by lactobacillus fermentum related to host iron absorption. Food Chem 2017;228:374–80.
[8] Yilmaz B, Li H. Gut microbiota and iron: the crucial actors in health and disease. Pharmaceuticals 2018;11(4):98.
[9] Malesza IJ, Bartkowiak-Wieczorek J, Winkler-Galicki J, Nowicka A, Dzięciołowska D, Błaszczyk M, et al. The dark side of iron: the relationship between iron, inflammation and gut microbiota in selected diseases associated with iron deficiency anaemia-a narrative review. Nutrients 2022;14(17):3478.

[10] McClorry S, Zavaleta N, Llanos A, Casapía M, Lönnerdal B, Slupsky CM. Anemia in infancy is associated with alterations in systemic metabolism and microbial structure and function in a sex-specific manner: an observational study. Am J Clin Nutr 2018;108(6):1238–48.
[11] Seo H, Yoon SY, ul-Haq A, Jo S, Kim S, Rahim MA, et al. The effects of iron deficiency on the gut microbiota in women of childbearing age. Nutrients 2023;15 (3):691.
[12] Ho TTB, Kumar A, Louis-Jacques AF, Dishaw LJ, Yee AL, Groer MW. The development of intestinal dysbiosis in anemic preterm infants. J Perinatol 2020;40 (7):1066–74.
[13] Yoon SY, Kim MJ, Lee MY, Kim KH, Lee N, Won JH. The effects of iron deficiency on the gut microbiota in young women. Blood 2022;140(Supplement 1):5348–9.
[14] Chen H, Wu W, Tang S, Fu R, Gong X, Hou H, et al. Altered fecal microbial and metabolic profile reveals potential mechanisms underlying iron deficiency anemia in pregnant women in China. Bosn J Basic Med Sci 2022;22(6):923–33.
[15] Soriano-Lerma A, García-Burgos M, Alférez MJM, Pérez-Carrasco V, Sanchez-Martin V, Linde-Rodríguez Á, et al. Gut microbiome-short-chain fatty acids interplay in the context of iron deficiency anaemia. Eur J Nutr 2022;61(1): 399–412.
[16] Dostal A, Chassard C, Hilty FM, Zimmermann MB, Jaeggi T, Rossi S, et al. Iron depletion and repletion with ferrous sulfate or electrolytic iron modifies the composition and metabolic activity of the gut microbiota in rats. J Nutr 2012;142 (2):271–7.
[17] Coe GL, Pinkham NV, Celis AI, Johnson C, DuBois JL, Walk ST. Dynamic gut microbiome changes in response to low-iron challenge. Appl Environ Microbiol 2021;87(3):2307–20.
[18] Mu Q, Kirby J, Reilly CM, Luo XM. Leaky gut as a danger signal for autoimmune diseases. Front Immunol 2017;8:598.
[19] Fine RL, Manfredo Vieira S, Gilmore MS, Kriegel MA. Mechanisms and consequences of gut commensal translocation in chronic diseases. Gut Microb 2020;11(2):217–30.
[20] Zheng L, Kelly CJ, Colgan SP. Physiologic hypoxia and oxygen homeostasis in the healthy intestine. A review in the theme: cellular responses to hypoxia. Am J Physiol Cell Physiol 2015;309(6):C350–60.
[21] Shao T, Zhao C, Li F, Gu Z, Liu L, Zhang L, et al. Intestinal hif-1α deletion exacerbates alcoholic liver disease by inducing intestinal dysbiosis and barrier dysfunction. J Hepatol 2018;69(4):886–95.
[22] Fachi JL, Felipe JdS, Pral LP, da Silva BK, Corrêa RO, de Andrade MCP, et al. Butyrate protects mice from clostridium difficile-induced colitis through an hif-1-dependent mechanism. Cell Rep 2019;27(3):750–61.
[23] Zhang H, Jamieson KL, Grenier J, Nikhanj A, Tang Z, Wang F, et al. Myocardial iron deficiency and mitochondrial dysfunction in advanced heart failure in humans. J Am Heart Assoc 2022;11(11):3.
[24] Li Y, Hansen SL, Borst LB, Spears JW, Moeser AJ. Dietary iron deficiency and oversupplementation increase intestinal permeability, ion transport, and inflammation in pigs. J Nutr 2016;146(8):1499–505.
[25] Din H, Yu X, Chen L, Han J, Zhao Y, Feng J. Tolerable upper intake levels of iron damage the intestine and alter the intestinal flora in weaned piglets. J Anim Sci 2020;12(9):1356–69.
[26] Pallarés I, Lisbona F, Aliaga IL, Barrionuevo M, Alférez MJM, Campos MS. Effect of iron deficiency on the digestive utilization of iron, phosphorus, calcium and magnesium in rats. Br J Nutr 1993;70(2):609–20.
[27] Reeves PG, Nielsen FH, Fahey Jr GC. Ain-93 purified diets for laboratory rodents: final report of the american institute of nutrition ad hoc writing committee on the reformulation of the ain-76a rodent diet. J Nutr 1993;123(11):1939–51.
[28] Beghini F, McIver LJ, Blanco-Míguez A, Dubois L, Asnicar F, Maharjan S, et al. Integrating taxonomic, functional, and strain-level profiling of diverse microbial communities with biobakery 3. Elife 2021;10:e65088.
[29] Yang S, Lin S, Kelen GD, Quinn TC, Dick JD, Gaydos CA, et al. Quantitative multiprobe pcr assay for simultaneous detection and identification to species level of bacterial pathogens. J Clin Microbiol 2002;40(9):3449–54.
[30] Supek F, Bošnjak M, Škunca N, Šmuc T. Revigo summarizes and visualizes long lists of gene ontology terms. PLoS One 2011;6(7):18.
[31] Walter W, Sánchez-Cabo F, Ricote M. Goplot: an r package for visually combining expression data with functional analysis. Bioinformatics 2015;31(17):2912–4.
[32] Tsuta K, Liu DC, Kalhor N, Wistuba, Moran CA. Using the mitosis-specific marker anti-phosphohistone h3 to assess mitosis in pulmonary neuroendocrine carcinomas. Am J Clin Pathol 2011;136(2):252–9.
[33] Zeng MY, Cisalpino D, Varadarajan S, Hellman J, Warren HS, Cascalho M, et al. Gut microbiota-induced immunoglobulin g controls systemic infection by symbiotic bacteria and pathogens. Immunity 2016;44(3):647–58.
[34] Rivera-Chávez F, Zhang Lillian F, Faber F, Lopez Christopher A, Byndloss Mariana X, Olsan Erin E, et al. Depletion of butyrate-producing clostridia from the gut microbiota drives an aerobic luminal expansion of salmonella. Cell Host Microbe 2016;19(4):443–54.
[35] Stronati L, Palone F, Negroni A, Colantoni E, Mancuso AB, Cucchiara S, et al. Dipotassium glycyrrhizate improves intestinal mucosal healing by modulating extracellular matrix remodeling genes and restoring epithelial barrier functions. Front Immunol 2019;10:939.
[36] Tao S, Xiong Y, Han D, Pi Y, Zhang H, Wang J. N-(3-oxododecanoyl)-l-homoserine lactone disrupts intestinal epithelial barrier through triggering apoptosis and collapsing extracellular matrix and tight junction. J Cell Physiol 2021;236(8): 5771–84.
[37] Semenza GL. Hif-1, o(2), and the 3 phds: how animal cells signal hypoxia to the nucleus. Cell 2001;107(1):1–3.
[38] Dilly AK, Lee YJ, Zeh HJ, Guo ZS, Bartlett DL, Choudry HA. Targeting hypoxia-mediated mucin 2 production as a therapeutic strategy for mucinous tumors. Transl Res 2016;169:19–30.
[39] Malinowska AM, Kok DE, Steegenga WT, Hooiveld GJEJ, Chmurzynska A. Human gut microbiota composition and its predicted functional properties in people with western and healthy dietary patterns. Eur J Nutr 2022;61(8):3887–903.
[40] Koh A, De Vadder F, Kovatcheva-Datchary P, Bäckhed F. From dietary fiber to host physiology: short-chain fatty acids as key bacterial metabolites. Cell 2016;165(6): 1332–45.
[41] Louis P, Flint HJ. Formation of propionate and butyrate by the human colonic microbiota. Environ Microbiol 2017;19(1):29–41.
[42] Stincone A, Prigione A, Cramer T, Wamelink MM, Campbell K, Cheung E, et al. The return of metabolism: Biochemistry and physiology of the pentose phosphate pathway. Biol Rev Camb Philos Soc 2015;90(3):927–63.
[43] Steinchen W, Zegarra V, Bange G. (p)ppgpp: Magic modulators of bacterial physiology and metabolism. Front Microbiol 2020;11:2072.
[44] Falà AK, Álvarez-Ordóñez A, Filloux A, Gahan CGM, Cotter PD. Quorum sensing in human gut and food microbiomes: significance and potential for therapeutic targeting. Front Microbiol 2022;13:1002185.
[45] Crittenden S, Cheyne A, Adams A, Forster T, Robb CT, Felton J, et al. Purine metabolism controls innate lymphoid cell function and protects against intestinal injury. Immunol Cell Biol 2018;96(10):1049–59.
[46] Cheng XR, Guan LJ, Muskat MN, Cao CC, Guan B. Effects of ejiao peptide-iron chelates on intestinal inflammation and gut microbiota in iron deficiency anemic mice. Food Funct 2021;12(21):10887–902.
[47] Vicentini FA, Keenan CM, Wallace LE, Woods C, Cavin J-B, Flockton AR, et al. Intestinal microbiota shapes gut physiology and regulates enteric neurons and glia. Microbiome 2021;9(1):210.
[48] Theocharis AD, Manou D, Karamanos NK. The extracellular matrix as a multitasking player in disease. FEBS J 2019;286(15):2830–69.
[49] Wright JA, Richards T, Srai SK. The role of iron in the skin and cutaneous wound healing. Front Pharmacol 2014;5:156.
[50] Kelly CJ, Zheng L, Campbell EL, Saeedi B, Scholz CC, Bayless AJ, et al. Crosstalk between microbiota-derived short-chain fatty acids and intestinal epithelial hif augments tissue barrier function. Cell Host Microbe 2015;17(5):662–71.
[51] Vedantam G, Hecht DW. Antibiotics and anaerobes of gut origin. Curr Opin Microbiol 2003;6(5):457–61.